NeuroImage 62 (2012) 1792–1799

Contents lists available at SciVerse ScienceDirect

NeuroImage

journal homepage: www.elsevier.com/locate/ynimg

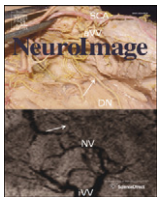

Full Length Articles

Architectural configuration and microstructural properties of the sacral plexus: A diffusion tensor MRI and fiber tractography study

Pasquelle K.N. van der Jagt [a,b], Pieter Dik [b], Martijn Froeling [c,d], Thomas C. Kwee [e], Rutger A.J. Nievelstein [e], Bennie ten Haken [a], Alexander Leemans [f,*]

[a] University of Twente, MIRA Institute for Biomedical Technology and Technical Medicine, Neuro Imaging, Enschede, The Netherlands
[b] Department of Pediatric Urology, University Children's Hospitals UMC Utrecht and AMC Amsterdam, Utrecht, The Netherlands
[c] Biomedical NMR, Department of Biomedical Engineering, Eindhoven University of Technology, Eindhoven, The Netherlands
[d] Department of Radiology, Academic Medical Center, University of Amsterdam, Amsterdam, The Netherlands
[e] Department of Radiology, University Medical Center Utrecht, Utrecht, The Netherlands
[f] Image Sciences Institute, University Medical Center Utrecht, Utrecht, The Netherlands

ARTICLE INFO

Article history:
Accepted 4 June 2012
Available online 13 June 2012

Keywords:
Diffusion tensor imaging
Fiber tractography
Sacral plexus
Peripheral nerves
Microstructural properties
Spina bifida

ABSTRACT

The ability to investigate microstructural properties of the central nervous system with diffusion tensor imaging (DTI) has been shown in many studies. More recently, DTI is being applied outside the brain showing promising results, for instance, for investigating muscle tissue. In this work, we demonstrate the feasibility of diffusion tensor imaging (DTI) and fiber tractography to study the nerves of the sacral plexus in humans in vivo and to assess the architectural configuration and microstructural properties of these peripheral nerves. For this research goal we optimized the acquisition parameters of a DTI sequence and acquired data from 10 healthy adults and one 12-year patient having spina bifida and neurogenic bladder dysfunction. For the healthy volunteers, we estimated the fractional anisotropy (FA) and mean (MD), axial (AD), and radial diffusivities (RD) of the sacral plexus nerves which may serve as a baseline for future studies. We demonstrated that tractography of the sacral plexus on a 3 Tesla MR scanner is feasible, giving 3D insight in the general anatomy and organization of the nerves L4 to S3. In addition, branches to the pudendal nerve were also found in 4 volunteers. There were no significant differences in any of the estimated diffusion measures between the right and left sided nerves or between the nerves L4 to S3 on an intra-subject basis. Furthermore, clinical feasibility of DTI and tractography in a child having spina bifida and neurogenic bladder dysfunction is demonstrated. The architectural configuration of the child's sacral plexus was comparable with the healthy volunteers and no significant disrupted nerve fibers were observed. However, there are strong indications that abnormal diffusion characteristics are present at the level of the neural tube defect due to incomplete segments of the nerves that are close to the vertebrae. These findings are encouraging for using DTI as a means to investigate changes in microstructural properties of the nerves of the sacral plexus. Moreover, this new methodology may provide a new avenue to a better analysis and diagnosis of neurogenic bladder dysfunctions.

Introduction

Diffusion tensor imaging (DTI) (Basser et al., 1994) has generated much enthusiasm because it is able to visualize the 3D architecture of white matter tracts and peripheral nerves non-invasively (Mori and Van Zijl, 2002; Tournier et al., 2011). In nerves, the magnitude of the displacement of water molecules due to random movement is larger along the fibers than in the perpendicular orientation (Moseley et al., 1990). This orientation dependence of diffusion is called anisotropy (Beaulieu, 2002) and can be quantified by applying diffusion-weighted acquisitions in multiple directions. The axis of preferred diffusion is characterized by the principal eigenvector and is considered to be oriented parallel to the fibers (Basser et al., 1994). This dominant diffusion orientation forms the basis of fiber tractography (FT), a technique that can virtually reconstruct fiber pathways from the underlying diffusion data (Basser et al., 2000; Conturo et al., 1999; Mori et al., 1999).

There is no doubt that DTI fiber tracking is providing new opportunities to study the anatomy of the central nervous system (Roberts and Schwartz, 2007). Although DTI is typically used for investigating white matter fiber pathways of the brain, other research areas are being explored opening new avenues for clinical in vivo applications. Fiber tracking of peripheral nerves is one of these fields (Hiltunen et al., 2005; Merlini et al., 2008, 2011; Takagi et al., 2009; Vargas et al., 2008, 2010). Recently, interest has been shown to image L5 and S1 lumbar nerves in healthy volunteers and patients suffering from disc herniation (Balbi et al., 2011). However, to the best of our knowledge, fiber tracking of the peripheral nerves L4, L5, S1, S2,

* Corresponding author at: Image Sciences Institute, University Medical Center Utrecht, Room Q0S.459, Heidelberglaan 100, Utrecht – 3584 CX, The Netherlands. Fax: +31 30 251 3399.
E-mail address: Alexander@isi.uu.nl (A. Leemans).

1053-8119/$ – see front matter © 2012 Elsevier Inc. All rights reserved.
doi:10.1016/j.neuroimage.2012.06.001

and S3 of the sacral plexus and estimating the fractional anisotropy (FA) and radial, axial, and mean diffusivities has never been done with a 3 Tesla MRI scanner before. With fiber tractography of the nerves of the sacral plexus, the anatomy and architectural fiber organization could be studied in vivo in patients, such as children having neurogenic bladder dysfunction due to congenital spinal or sacral anomalies. In these patients, for instance, the exact mechanism of disturbed innervation of the bladder is not known and novel techniques, such as DTI and fiber tractography, could improve our understanding on this matter.

In this work, we demonstrate the feasibility of DTI and fiber tractography of the nerves of the sacral plexus in healthy volunteers. The fractional anisotropy (FA), mean diffusivity (MD), axial diffusivity (AD), and radial diffusivity (RD) of nerves L4 to S3 are estimated in ten healthy volunteers. In addition, the clinical feasibility of DTI and fiber tractography is evaluated in a child having spina bifida and neurogenic bladder dysfunction. Preliminary findings of this research were presented at the 8th annual world congress of IBMISPS on brain, spinal cord mapping and image guided therapy in San Francisco.

Materials and methods

Data acquisition

Local institutional review board approval was obtained for this study and written informed consent was given by all subjects prior to the MR examination. Ten healthy volunteers [4 men, 6 women, mean age 24 years (range 22–29 years)] underwent a scan of the sacral plexus. More specifically, MR imaging was performed from the level of the L4 nerve to the inguinal region, including the first part of the sciatic nerve. Furthermore, one 12 year old boy with neurogenic bladder dysfunction was included, after informed consent was obtained from him and his parents. At birth he was diagnosed with spina bifida with neural tube defect located at the lumbosacral L5–S1 level. Closure of the neural tube defect was performed right after he was born and his motor and sensible sense is intact up to the level of S1. He had severe neuropathic bladder problems and for this he needed bladder augmentation in the past. He performs intermittent catheterization of the bladder 5 times

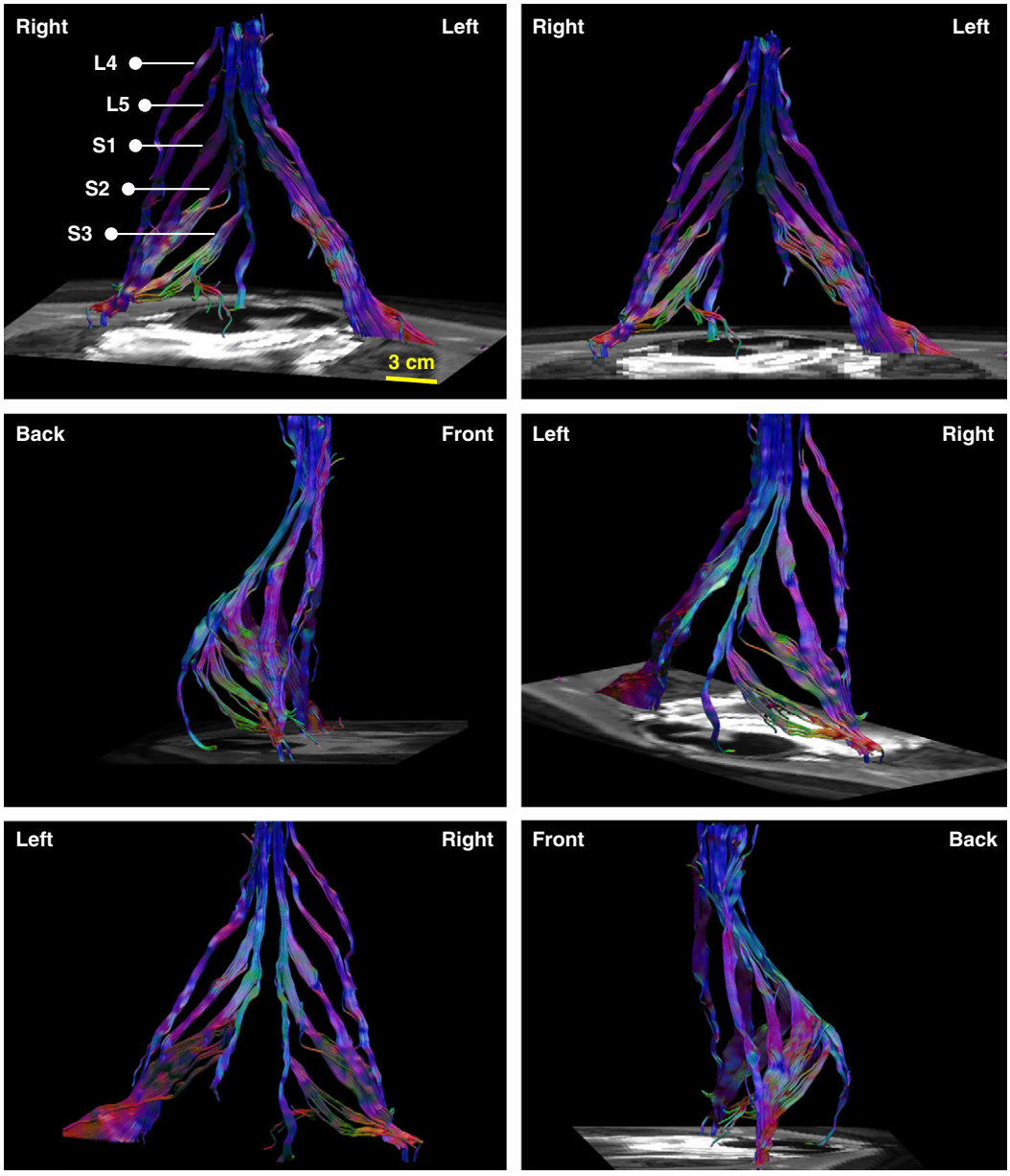

Fig. 1. Architectural configuration of the reconstructed fiber bundles L4 to S3 in one volunteer as seen from six different views.

per day and with these measures he is dry with a bladder volume of 450 cc. He is able to walk. Before the MRI examination, subjects were asked to go to the toilet to ensure an empty bladder, as stored urine gave disturbance on the DW images.

All subjects were examined with a 3.0-T MR system (Achieva; Philips Healthcare, Best, The Netherlands) using a 16-channel phased-array surface coil. First, a monopolar Stejskal–Tanner diffusion weighting pulse sequence was used with parameters according to the guidelines presented in Jones and Leemans, 2011. DTI was performed with diffusion-weighted spin echo single-shot echo planar imaging (EPI) in the axial plane with the following parameters; TE = 44 ms, TR = 9683 ms, SENSE factor 2, number of excitations = 2, FOV 288 × 204 mm^2, matrix size 96 × 68, 55 slices with thickness = 3.0 mm, resulting in a voxel size of 3.0 × 3.0 × 3.0 mm^3, SENSE factor 2, half scan 0.6, EPI train length (ETL): 25, EPI frequency bandwidth = 3621 Hz, G = 62 mT/m, Δ/δ = 21.5/13.0 ms, SPAIR fat suppression with inversion delay = 83 ms and TR = 176 ms, *b*-values 0 en 800 s/mm^2, and 15 gradient directions that are distributed uniformly on the unit sphere (Jones et al., 1999). The total acquisition time of the DTI sequence was 11:46 min. In addition, a 3D Turbo Spin Echo (3D-TSE) scan was acquired with parameters: TR = 3000 ms, TE = 286, TSE factor 180, startup echoes 4, FOV 250 × 250 × 100 mm^2, slice orientation is coronal, matrix size 250 × 250 × 100, reconstruction matrix 512 × 512 × 200, resulting in a voxel size of 0.49 × 0.49 × .5 mm^3, number of excitations 2, SENSE factor 2, SPAIR fat suppression with inversion delay = 240 ms and TR = 3000 ms, total acquisition time 10:03 min. Finally, a diffusion-weighted imaging with background body signal suppression (DWIBS) scan was acquired with an inversion recovery echo planar imaging (IR-EPI) sequence and the following parameters: slice orientation is axial, TR = 8900 ms, TE = 53 ms, TI = 260 ms, FOV 375 × 254 mm, matrix size 124 × 85, Reconstruction matrix 256 × 256, 40 slices with thickness = 4.0 mm, resulting in a voxel size of 1.5 × 1.5 × 4.0 mm^3, b-value = 0, 600, 800 and 1000 s/mm^2, Δ/δ = 26.0/18.2 ms, EPI train length 47, number of excitations 3, SENSE factor 2, total acquisition time 10:05 min.

Data processing and analyses

The DTI datasets were post-processed using the *ExploreDTI* diffusion MRI toolbox (www.ExploreDTI.com) (Leemans et al., 2009). Color encoding of the reconstructed fiber pathways was chosen according to the standardized color code used in brain studies: blue indicating the cephalo-caudal, red indicating the left–right and green indicating the antero-posterior direction. The following multi-step procedure was applied to analyze and process the data; (a) Subject motion and eddy-current induced geometrical distortions were corrected (Leemans and Jones, 2009), (b) the diffusion tensors and subsequently the FA, MD, AD and RD were calculated using a non-linear regression procedure, and (c) a standard deterministic streamline tractography approach was used, as described in Basser et al. (2000), to reconstruct the fiber pathways of interest. Seed regions-of-interest (ROIs) were placed at different levels of the spinal cord nerves. More specifically, the seed ROIs were placed in the middle of each tract-of-interest, accompanied by "AND" selection ROIs at both ends of the nerve tract (Conturo et al., 1999). A very low FA threshold (0.001) was defined to minimize false negatives, the angle threshold was 30°, and the step size was set to 1 mm. Note that despite the virtually non-existing FA threshold, the angle threshold of 30 degrees in combination with the multiple "AND" ROIs provided a robust and reproducible procedure to reconstruct the fiber pathways of interest (see Fig. A of supplementary material). Evaluation of the DTI images and fiber tractography results included identification of the anatomy and 3D organization of the fibers structures of the sacral plexus. Feasibility of tracking of the pudendal nerve is evaluated as well, as this nerve innervates the external urethral sphincter, which is of interest for our patient case study. Finally, for the healthy volunteers the microstructural characteristics, as reflected by the DTI metrics FA, MD, AD, and RD, were estimated for each side for the nerves L4 to S3.

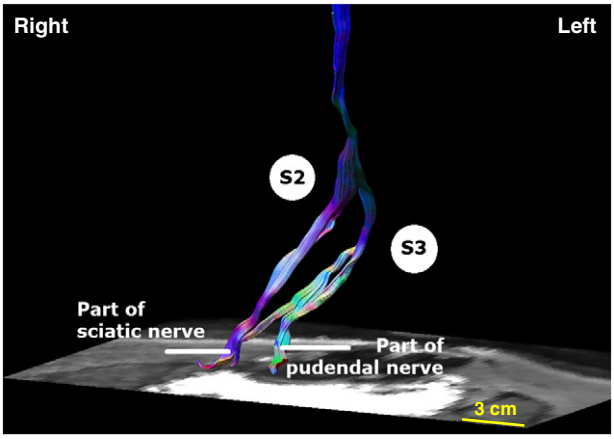

Fig. 2. S2 and a branch of S3 running to a part of the sciatic nerve. Furthermore, it can be seen that a branch of S3 forms a part of the pudendal nerve.

Statistical evaluation

The FA, MD, AD and RD values of the nerves L4 to S3 of the healthy volunteers were compared between the left and the right side using a non-parametric Mann–Whitney U test. Furthermore, with the non-parametric Kruskall-Wallis test any potential differences in these diffusion measures between the individual nerves were investigated. A

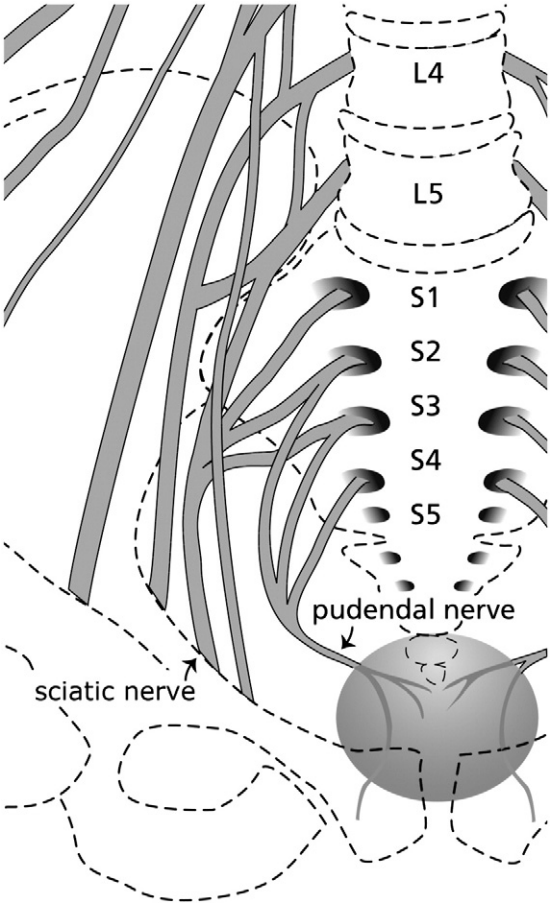

Fig. 3. Normal anatomy as known from cadaver studies. Good agreement can be seen between the known anatomy and the branching of S3 to the pudendal nerve as shown in Fig. 2.

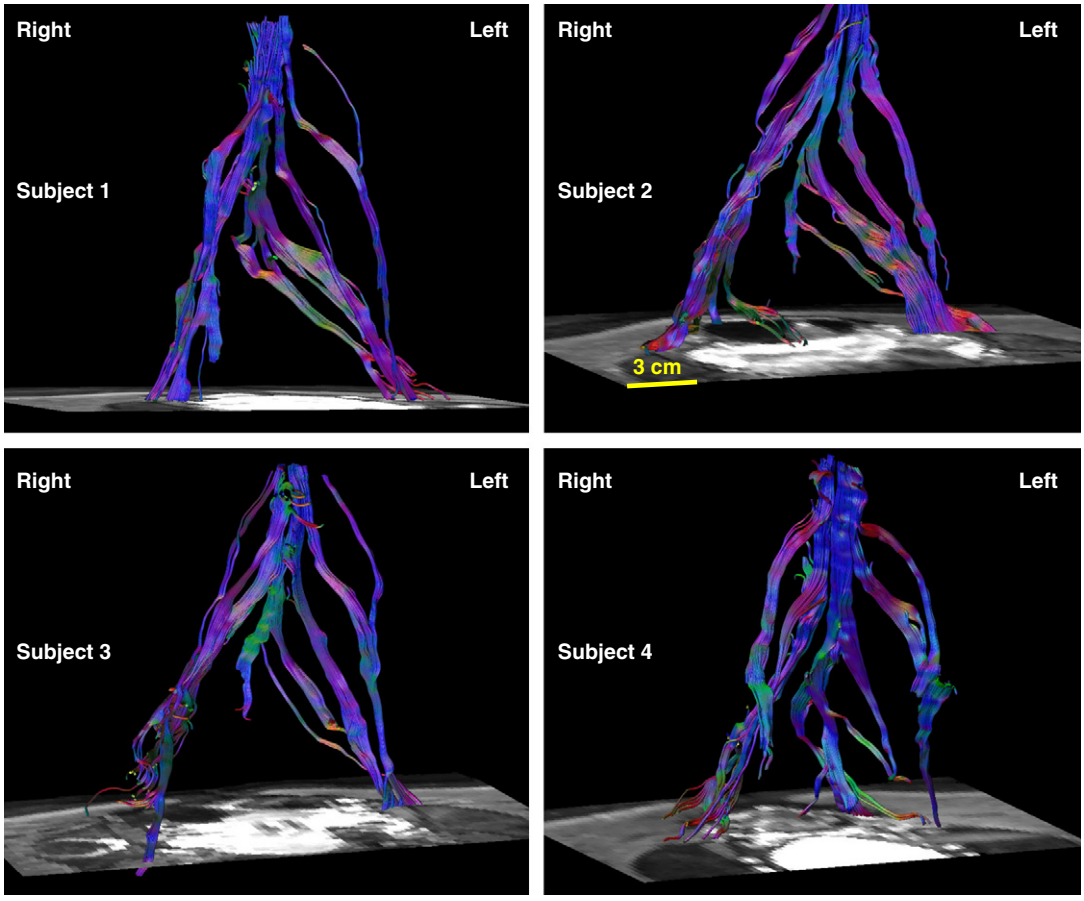

Fig. 4. Feasibility of tractography of the normal sacral plexus is demonstrated in four different volunteers.

p-value <0.05 was considered significant. The analysis was performed using the software of SPSS version 15.0 (SPSS Inc., Chicago, IL).

Results

Tractography results of healthy volunteers

Fiber tractography of the sacral plexus was feasible in all ten healthy volunteers. The roots and trunks of the sacral plexus were identified bilaterally. Tractography of the nerves of the sacral plexus gave 3D insights in the normal anatomy of the reconstructed fiber pathways. The architectural configuration of the fibers was comparable in all healthy volunteers. Similarity was found in the characteristics of the sacral plexus regarding anatomy, organization and branching of the fibers bilaterally. Furthermore, tractography clearly visualized how the different nerves arose from the spinal cord and ran into the periphery. The architectural configuration of one volunteer is demonstrated in Fig. 1, where six different views are shown (for the corresponding FA color-encoded image, the reader is referred to Fig. B in the supplementary material). In 4 volunteers, the nerves of the sacral plexus could be tracked from L4 to S3. In two volunteers, L4 could not be tracked reliably on one side. In the remaining four volunteers, the sacral plexus was tracked from L5 to S3 bilaterally, from L4 to S2 bilaterally, from L5 to S2 bilaterally, and from L4 to S3 without S2 and S3 on one side. S4 could not be tracked reliably in all volunteers. However, in 4 volunteers, branches to the pudendal nerve were found. Fig. 2 shows how S2 and a branch of S3 run to a part of the sciatic nerve and how fibers of the S3 branch form a part of the pudendal nerve. Agreement is found with known anatomy, as illustrated with the schematic overview in Fig. 3. To demonstrate the inter-subject reproducibility, tractography results of the normal sacral plexus are shown in Fig. 4 for four different volunteers.

Microstructural parameters of healthy volunteers

FA, MD, AD and RD measurements were obtained for each individual nerve from L4 to S3 and for each side, separately. As there were no significant differences between the left and the right side (all $p>0.05$), both sides were pooled for each nerve and summarized (average across ten subjects) in Table 1. Further analysis revealed that there were no significant differences between the individual nerves (all $p>0.05$).

Table 1
Mean (±SD) fractional anisotropy (FA), mean/axial/radial (MD/AD/RD) diffusivity, and approximate length/volume of the individual nerves of the ten healthy volunteers.

Nerve	FA	Diffusivity (mm^2/s) $\times 10^{-3}$			Tract length (mm)	Tract volume (mm^3)
		MD	AD	RD		
L4	0.28 (±0.05)	1.34 (±0.23)	1.73 (±0.24)	1.15 (±0.22)	110 (±39)	4860 (±2133)
L5	0.31 (±0.03)	1.42 (±0.21)	1.86 (±0.24)	1.19 (±0.20)	143 (±54)	6426 (±1944)
S1	0.26 (±0.03)	1.83 (±0.24)	2.31 (±0.27)	1.59 (±0.22)	139 (±45)	7560 (±4596)
S2	0.23 (±0.03)	1.72 (±0.30)	2.12 (±0.37)	1.52 (±0.27)	126 (±54)	7601 (±5191)
S3	0.22 (±0.03)	1.62 (±0.32)	1.98 (±0.39)	1.43 (±0.29)	148 (±66)	6561 (±4104)

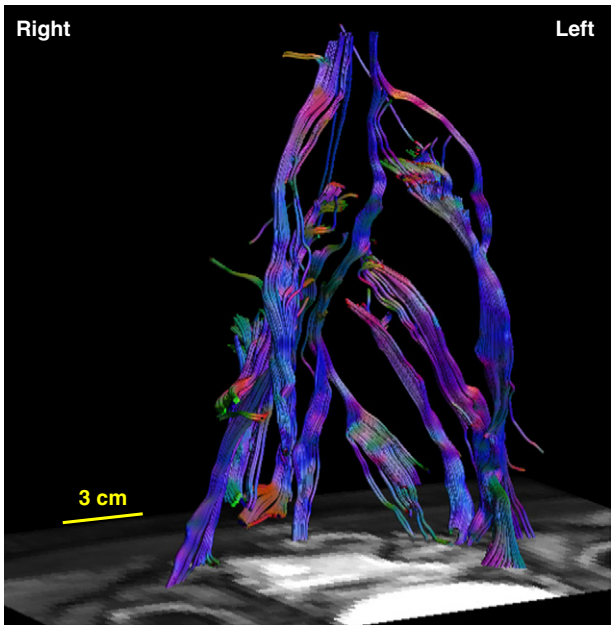

Fig. 5. Anatomy and organization of the fiber pathways in the boy with spina bifida.

The overall mean and standard deviation (SD) of all nerves (pooled across left/right side and across subjects) is for FA 0.25 ± 0.05 and for MD, AD and RD, $1.61*10^{-3} \pm 0.33*10^{-3}$, $2.02*10^{-03} \pm 0.38*10^{-3}$, and $1.40*10^{-3} \pm 0.30*10^{-3}$ mm^2/s, respectively.

Tractography results of child with spina bifida

Fiber tractography of the nerves of the sacral plexus in a child with spina bifida was feasible and provided a plausible anatomy of the 3D fiber organization (Fig. 5). Although all nerve roots L4 to S3 were found bilaterally and the architectural configuration was comparable with the healthy volunteers, it was impossible to track all fiber segments of L5 to S2. More specifically, the parts most adjacent to the vertebra could not be reconstructed given the predefined fiber tractography parameter thresholds. The tracking results for S1, for instance, are visualized in Fig. 6. Note that this phenomenon was present bilaterally, but more prominent on the right side (Fig. 7). For comparison, the anatomical TSE and DWIBS images are shown in Figs. 8 and 9, respectively.

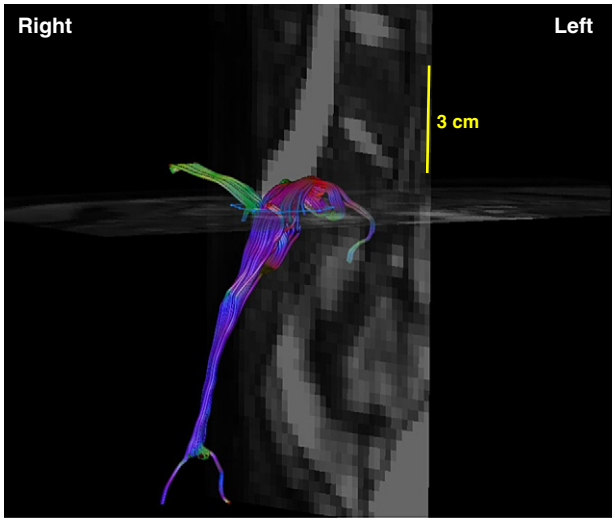

Fig. 6. Incomplete reconstruction of the fiber pathways of S1 in the boy with spina bifida.

Discussion

To the best of our knowledge, this is the first study that demonstrates the feasibility of DTI and fiber tractography for investigating the nerves of the sacral plexus in healthy adults with a 3 Tesla MRI scanner. Fiber tracking provided clear insights in the normal anatomy and architectural organization of the sacral plexus and its branching nerves, and corresponded to their known anatomy. Quantification of these nerves was provided by estimating the FA, MD, AD and RD reflecting the microstructural characteristics of the normal peripheral nerves. Finally, we presented fiber tractography results of the sacral plexus in a boy with spina bifida and neurogenic bladder dysfunction.

Tractography is an advanced technique to reconstruct nerve fibers in vivo and non-invasively. However, the technique is difficult to validate due to lack of a gold standard. Fiber tracking reliability also depends on the quality of the data and on the robustness of the algorithms used (Jeurissen et al., 2011; Tournier et al., 2002). Acquisition of high-quality images, however, is time consuming and in clinical practice, quality is usually compromised to allow shorter scan times. Nevertheless, considerable efforts have been made to optimize the acquisition protocol for high quality datasets. The echo train length was kept as short as possible. This minimizes the T2* signal decay resulting in a higher SNR, which is the most important parameter in DTI for accurate fiber tractography and DTI parameter measurements (Hiltunen et al., 2005; Vargas et al., 2010). Furthermore, the gradient directions were distributed uniformly on the unit sphere (Jones and Leemans, 2011). To retain an acceptable acquisition time only 15 gradient directions were used with a NSA of 2. This was preferred above the use of 32 gradient directions and a NSA of 1. However, with a relatively large voxel size of $3 \times 3 \times 3$ mm^3, partial volume effects could not be avoided in the smaller nerves of the plexus (Alexander et al., 2001). It is important to realize that voxel size changes the degree with which partial volume effects occur and that intrinsic fiber tract features, such as their curvature and volume, can affect the estimation of diffusion tensor metrics (Vos et al., 2011).

With the MD ranging from $1.34*10^{-3}$ to $1.83*10^{-3}$ and the FA ranging from 0.21 to 0.31, our results confirm that the MD is higher and the FA is lower in these peripheral nerves than in brain tissue (Lee et al., 2009). This is in line with an expected higher rate of diffusion in less compact tissue. Noteworthy is the trend in lower FA for S1 to S3 compared to L4 and L5. This is confirmed by the relatively higher AD values in these nerves. As the L4 and L5 nerves are thicker than the S2 and S3 nerves (Hogan, 1996), there may be a modulation caused by partial voluming effects (Vos et al., 2011). By contrast, however, S1 is thicker than L4 and L5 (Hogan, 1996), but its FA is lower and its AD is higher than those of L4 and L5. It is therefore plausible that other factors could cause these differences, such as membrane permeability, axonal density, and packing configuration, among others reflecting true microstructural differences between lumbar and sacral nerves (Song et al., 2002).

In a recent study by Vargas et al., the feasibility of DTI and tractography was investigated in the brachial plexus. They found a mean MD of 1.70 ± 0.35 $*10^{-3}$ mm^2/s and a mean FA of 0.30 ± 0.079 in normal brachial fibers C5 to C8 (Vargas et al., 2010). Their results correspond well with our data. In another study, Hiltunen et al. found MD values for the tibial and peroneal nerves varying from $0.97*10^{-3}$ to $1.56*10^{-3}$ mm^2/s and in the nerves of the wrist varying from $0.71*10^{-3}$ to $1.36*10^{-3}$ mm^2/s (Hiltunen et al., 2005). Overall these MD values are somewhat lower than our measured MDs. This could be attributed to the higher b-value that was used in their study ($b = 1000$ s/mm^2). Finally, in a study of Balbi et al. a FA of 0.22 ± 0.01 is found in L5 and S1, which is comparable to the data in our study. In

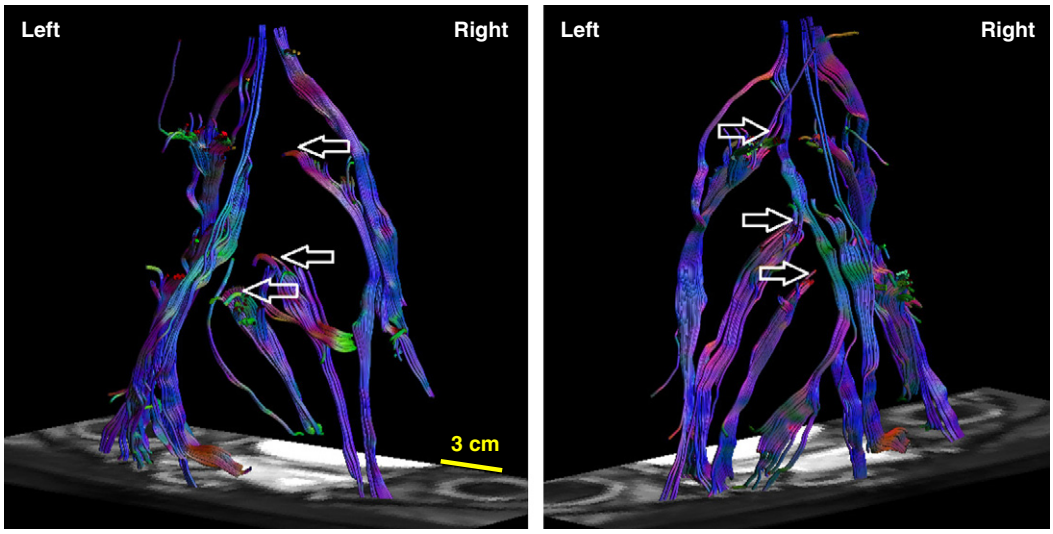

Fig. 7. Two different views of the fiber tractography results in the boy with spina bifida. The apparently missing segments at the level of root ascension in L5 to S2 are indicated with arrows.

addition, they observed an MD of 1.85 ± 0.13 (Balbi et al., 2011), which seems to be larger than our data values. This discrepancy may well be due to the higher age of the volunteers, the difference in b-value, and/or more diffusion gradients (Balbi et al., 2011).

In addition to the FA and MD, we also estimated the AD and RD of the lumbar and sacral nerves. To the best of our knowledge, this is the first study that has calculated these measures for such peripheral nerves. In a study by Wheeler-Kingshott et al., the AD and RD were computed for the cervical spinal cord. They measured an AD of $1.77 \pm 0.02 * 10^{-3}$ in C2 and C3, and an AD of $1.60 \pm 0.09 * 10^{-3}$ in C5 and C6 (Wheeler-Kingshott et al., 2002). Furthermore, they found an RD of $0.56 \pm 0.01 * 10^{-3}$ in C2 and C3, and $0.59 \pm 0.03 * 10^{-3}$ in C5 and C6 (Wheeler-Kingshott et al., 2002), which are lower compared to the values obtained in our study. In addition to the possibility of measuring genuine differences in microstructural tissue organization, heterogeneity of subject/patient groups and acquisition settings may be the cause of these differences. The investigation of the RD and providing a reference value for the nerves of the sacral plexus may prove to be of great value as previous research has indicated that the RD may be related to demyelinization (Song et al., 2002).

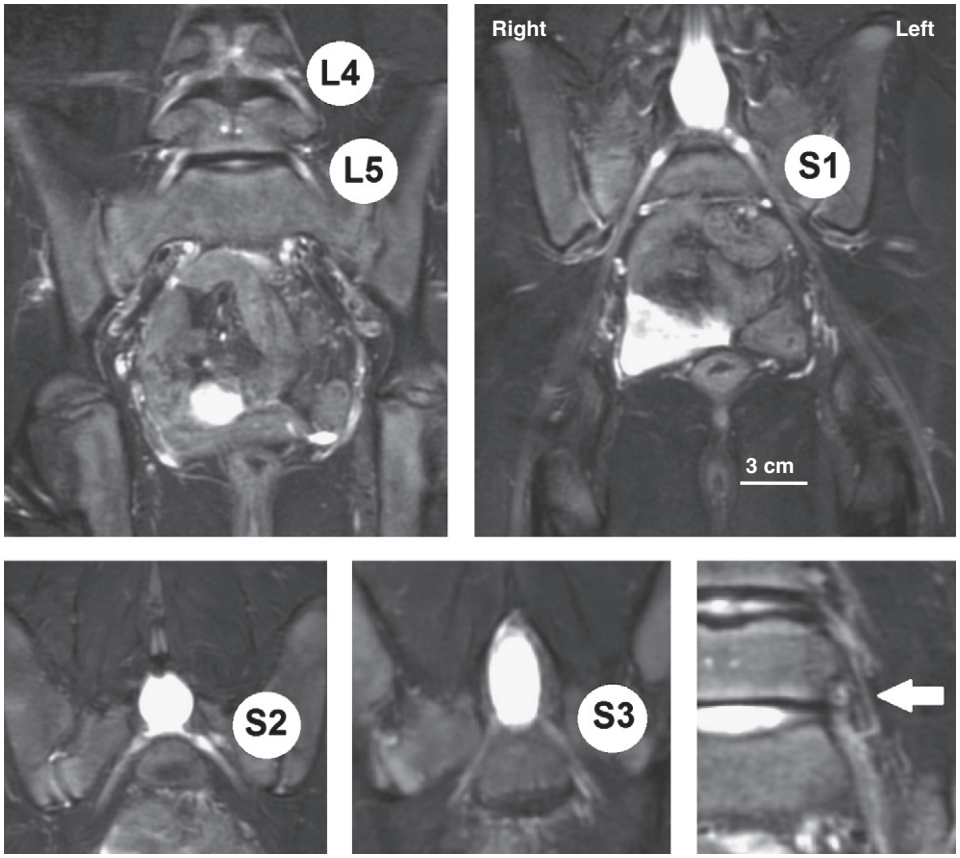

Fig. 8. Visualization of the nerves L4, L5, S1, S2, and S3 of the sacral plexus on the TSE scan. The arrow in the lower right image indicates the small contribution of L4 in the lumbosacral trunk.

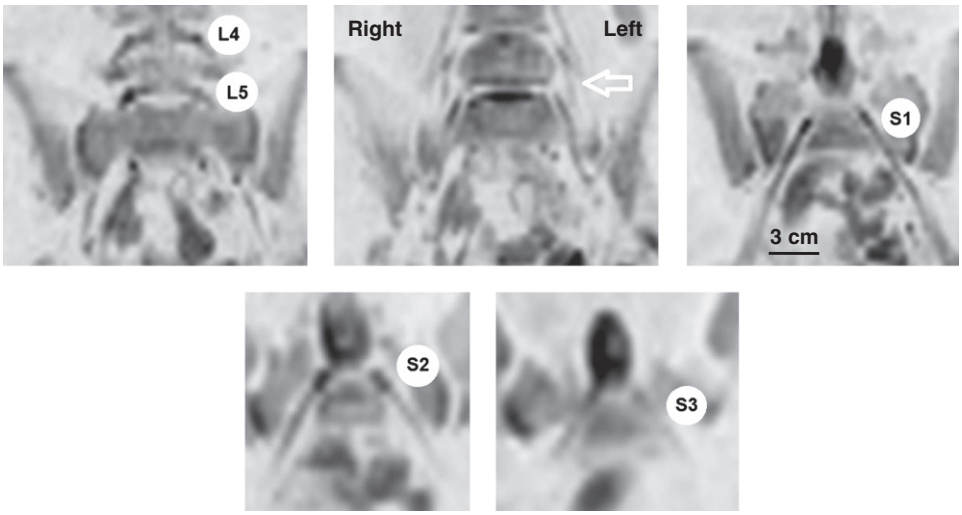

Fig. 9. Visualization of the nerves L4, L5, S1, S2, and S3 of the sacral plexus on the DWIBS scan. The arrow in the top middle image indicates the lumbosacral trunk.

Apart from the healthy subjects, we also scanned a young patient with spina bifida and neurogenic bladder dysfunction. Despite the absence of any statistically significant difference in any of the diffusion values and for any of the nerves, the tractography results of this subject showed abnormal configurations in the sacral nerve roots L5 to S2, in correspondence with the level of the boy's neural tube defect. At first instance, these untrackable segments could be explained by motion artifacts. However, this is contradicted by the fact that in the more distal trajectories of the peripheral nerves L5 to S2, fiber tractography could still easily be performed. Consequently, it may well be the case that the underlying microstructural anomalies related to the neurogenic bladder dysfunction itself could be the cause of the untrackable segments. Further research with large patient populations and age matched controls is needed to confirm these findings, but this example is already encouraging for bringing DTI closer to the clinical realm of urological disorders. Only then, it will become clear whether DTI can provide new insights in the etiology of, for instance, neurogenic bladder dysfunction or whether DTI can bring an added value in the work-up of spina bifida patients that are eligible for neuro-anastomoses.

It is important to acknowledge the limitations of DTI. It should be clear that DTI based on single-shot EPI is susceptible to motion artifacts and geometrical distortions, and can only provide data at a relatively low resolution. Despite the applied motion-distortion correction to the data, FA measurements could still be affected by residual misalignments due to nonlinear behavior of these artifacts. In addition, confounds caused by partial volume effects may be larger for the smaller nerves, which could also explain the lower FA values measured in these nerves (Hiltunen et al., 2005; Jeurissen et al., in press; Tournier et al., 2011; Vargas et al., 2010; Vos et al., 2011). Although it appears that DTI parameters estimated from tractography are more reliable than those calculated by placing ROIs (Van Hecke et al., 2008), their interpretation may still be non-trivial as shown in previous work (Vos et al., 2012; Wheeler-Kingshott and Cercignani, 2009). The observed abnormalities for the patient with neurogenic bladder dysfunction presented in this work should be interpreted with great care as the incomplete fiber reconstructions may also be partly caused by imperfections in the data or the imaging technique itself. In this context, it should be obvious that DTI cannot or should not replace anatomical plexus imaging using 2D T1- and T2-weighted sequences or with high resolution 3D TSE protocols, but that it can offer valuable complementary information.

Conclusions

This paper presents the first study showing the feasibility of DTI and fiber tractography for quantifying microstructural properties (FA, MD, AD, RD) of the nerves of the sacral plexus in healthy adults. We have demonstrated that fiber tracking allows for 3D insights in the normal anatomy and general organization of the sacral plexus and its branching nerves. In addition, we provided FA, MD, AD and RD values of ten healthy subjects which may serve as a baseline for future studies that may involve pathology. Finally, we have given an example that shows the feasibility of DTI and fiber tractography for investigating the sacral plexus in a clinical setting, by investigating a boy with spina bifida and neurogenic bladder dysfunction.

Supplementary data to this article can be found online at http://dx.doi.org/10.1016/j.neuroimage.2012.06.001.

References

Alexander, A.L., Hasan, K.M., Lazar, M., Tsuruda, J.S., Parker, D.L., 2001. Analysis of partial volume effects in Diffusion-Tensor MRI. Magn. Reson. Med. 45, 770–780.
Balbi, V., Budzik, J.F., Duhamel, A., Bera-Louville, A., Le Thuc, V., Cotton, A., 2011. Tractography of lumbar nerve roots: initial results. Eur. Radiol. 21, 1153–1159.
Basser, P.J., Mattiello, J., LeBihan, D., 1994. MR diffusion tensor spectroscopy and imaging. Biophys. J. 66, 259–267.
Basser, P.J., Pajevic, S., Pierpaoli, C., Duda, J., Aldroubi, A., 2000. In vivo fiber tractography using DT-MRI data. Magn. Reson. Med. 44, 625–632.
Beaulieu, C., 2002. The basis of anisotropic water diffusion in the nervous system — a technical review. NMR Biomed. 15, 435–455.
Conturo, T.E., Lori, N.F., Cull, T.S., Akbudak, E., Snyder, A.Z., Shimony, J.S., McKinstry, R.C., Burton, H., Raichle, M.E., 1999. Tracking neuronal fiber pathways in the living human brain. Proc. Natl. Acad. Sci. 96, 10422–10427.
Hiltunen, J., Suortti, T., Arvela, S., Seppa, M., Joensuu, R., Hari, R., 2005. Diffusion tensor imaging and tractography of distal peripheral nerves at 3 T. Clin. Neurophysiol. 116, 2315–2323.
Hogan, Q., 1996. Size of human lower thoracic and lumbosacral nerve roots. Anesthesiology 85, 37–42.
Jeurissen, B., Leemans, A., Jones, D.K., Tournier, J.-D., Sijbers, J., 2011. Probabilistic fiber tracking using the residual bootstrap with constrained spherical deconvolution. Hum. Brain Mapp. 32, 461–479.
Jeurissen, B., Leemans, A., Tournier, J.-D., Jones, D.K., and Sijbers, J., in press. Investigating the prevalence of complex fiber configurations in white matter tissue with diffusion MRI. Hum. Brain Mapp doi:10.1002/hbm.22099. [Epub ahead of print]
Jones, D.K., Leemans, A., 2011. Diffusion tensor imaging. Methods Mol. Biol. 711, 127–144.
Jones, D.K., Horsfield, M.A., Simmons, A., 1999. Optimal strategies for measuring diffusion in anisotropic systems by magnetic resonance imaging. Magn. Reson. Med. 42, 515–525.
Lee, C.E., Danielian, L.E., Thomasson, D., Baker, E.H., 2009. Normal regional fractional anisotropy and apparent diffusion coefficient of the brain measured on a 3 T MR scanner. Neuroradiology 51, 3–9.
Leemans, A., Jones, D.K., 2009. The B-matrix must be rotated when correcting for subject motion in DTI data. Magn. Reson. Med. 61, 1336–1349.
Leemans, A., Jeurissen, B., Sijbers, J., Jones, D.K., 2009. ExploreDTI: a graphical toolbox for processing, analyzing, and visualizing diffusion MR data. 17th Annual Meeting of Intl Soc Mag Reson Med, Hawaii, USA, p. 3537.
Merlini, L., Viallon, M., De Coulon, G., Lobrinus, J.A., Vargas, M.I., 2008. MRI neurography and diffusion tensor imaging of a sciatic perineuroma in a child. Pediatr. Radiol. 38, 1009–1012.

Merlini, L., Vargas, M.I., Anooshiravani, M., Viallon, M., Fluss, J., Hanquinet, S., 2011. Look for the nerves! MR neurography adds essential diagnostic value to routine MRI in pediatric practice: a pictorial overview. J. Neuroradiol. 38, 141–147.

Mori, S., van Zijl, P.C., 2002. Fiber tracking: principles and strategies - a technical review. NMR Biomed. 15, 468–480.

Mori, S., Crain, B.J., Chacko, V.P., van Zijl, P.C., 1999. Three-dimensional tracking of axonal projections in the brain by magnetic resonance imaging. Ann. Neurol. 45, 265–269.

Moseley, M.E., Cohen, Y., Kucharczyk, J., Mintorovitch, J., Asgari, H.S., Wendland, M.F., Tsuruda, J., Norman, D., 1990. Diffusion-weighted MR imaging of anisotropic water diffusion in cat central nervous system. Radiology 176, 439–445.

Roberts, T.P., Schwartz, E.S., 2007. Principles and implementation of diffusion-weighted and diffusion tensor imaging. Pediatr. Radiol. 37, 739–748.

Song, S.K., Sun, S.W., Ramsbottom, M.J., Chang, C., Russell, J., Cross, A.H., 2002. Dysmyelination revealed through MRI as increased radial (but unchanged axial) diffusion of water. Neuroimage 17, 1429–1436.

Takagi, T., Nakamura, M., Yamada, M., Hikishima, K., Momoshima, S., Fujiyoshi, K., Shibata, S., Okano, H.J., Toyama, Y., Okano, H., 2009. Visualization of peripheral nerve degeneration and regeneration: monitoring with diffusion tensor tractography. Neuroimage 44, 884–892.

Tournier, J.D., Calamante, F., King, M.D., Gadian, D.G., Connelly, A., 2002. Limitations and requirements of diffusion tensor fiber tracking: an assessment using simulations. Magn. Reson. Med. 47, 701–708.

Tournier, J.D., Mori, S., Leemans, A., 2011. Diffusion tensor imaging and beyond. Magn. Reson. Med. 65, 1532–1556.

Van Hecke, W., Leemans, A., Sijbers, J., Vandervliet, E., Van Goethem, J., Parizel, P.M., 2008. A tracking-based diffusion tensor imaging segmentation method for the detection of diffusion-related changes of the cervical spinal cord with aging. J. Magn. Reson. Imaging 27, 978–991.

Vargas, M.I., Delavelle, J., Jlassi, H., Rilliet, B., Viallon, M., Becker, C.D., Lovblad, K.O., 2008. Clinical applications of diffusion tensor tractography of the spinal cord. Neuroradiology 50, 25–29.

Vargas, M.I., Viallon, M., Nguyen, D., Delavelle, J., Becker, M., 2010. Diffusion tensor imaging (DTI) and tractography of the brachial plexus: feasibility and initial experience in neoplastic conditions. Neuroradiology 52, 237–245.

Vos, S.B., Jones, D.K., Viergever, M.A., Leemans, A., 2011. Partial volume effect as a hidden covariate in DTI analyses. Neuroimage 55, 1566–1576.

Vos, S.B., Jones, D.K., Jeurissen, B., Viergever, M.A., Leemans, A., 2012. The influence of complex white matter architecture on the mean diffusivity in diffusion tensor MRI of the human brain. Neuroimage 59, 2208–2216.

Wheeler-Kingshott, C.A., Cercignani, M., 2009. About "axial" and "radial" diffusivities. Magn. Reson. Med. 61, 1255–1260.

Wheeler-Kingshott, C.A., Hickman, S.J., Parker, G.J., Ciccarelli, O., Symms, M.R., Miller, D.H., Barker, G.J., 2002. Investigating cervical spinal cord structure using axial diffusion tensor imaging. Neuroimage 16, 93–102.